INVESTIGATION ON THE OXIDATIVE CAPACITY OF Zn MODIFIED Mn_3O_4 NANOPARTICLES BY PHOTOCATALYTIC METHYLENE BLUE DYE DEGRADATION

G. SRILATHA[a], P. MURALIMANOHAR[a], K. SATHYAMOORTHY[a], P. VINOTHKUMAR[a], S. SRIRAM[b], M. PRIYA[a,*]

[a]*Department of Physics,Saveetha Engineering College,Thandalam,Chennai, India*

[b]*Department of Physics, School of Electrical & Electronics Engineering, SASTRA University, Thanjavur, India*

Pure and Zn doped manganese (II, III) oxide (Mn_3O_4) nanoparticles were prepared by simple chemical precipitation method at room temperature with different atomic percentages (6, 12, 18) of Zn. The obtained products were subjected to various characterizations namely powder X-ray diffraction (XRD), microstructure and morphology were investigated by scanning and transmission electron microscopy (SEM and TEM), element analysis was done by energy-dispersive X-ray spectroscopy (EDX). Specific surface area of all the samples were measured by Brunauer–Emmett–Teller (BET) analysis. The optical absorption (UV-vis) property of the samples, confirmed electronic transitions and increase in the band gap of the products. The as-synthesized samples were used for degrading methylene blue (MB) dye of which 12at% Zn in Mn_3O_4 showed best oxidation efficiency compared to other samples.

(Received April 15, 2020; Accepted September 3, 2020)

Keywords: Mn_3O_4 nanoparticles, Oxidation competency, Methylene blue

1. Introduction

Manganese oxides as transition metal oxides are turning out to be one of the most notable and myriad classes of functional materials that are having a key impact on applied science [1-2]. In the present areas of research it has wide applications as catalysts [3-5], rechargeable batteries [6], magneto-electronic devices [7], sensors [8, 9], and as electrochemical capacitors [10–12]. In the domain of environmental pollution caused by dyes, the heterogeneous photocatalytic process is an undisputed technique, which can be triumphantly used to oxidize the organic dyes present in the effluents. Experimental investigations reveal that by photocatalytic process almost complete mineralization of organic compounds to inorganic anions, carbon dioxide and water [13-15] takes place. Many alterations are carried out by various research groups by doping catalysts with metals, non-metals or co-doping with metals and non-metals or by coupling with others semiconductor materials, metal complexes, encapsulation of dyes [16-26] etc.. Among the various forms of manganese oxides, Mn_3O_4 is a semiconductor, its inherent nature of being non-toxic and chemically stable, makes it more favourable for being used as a photocatalyst. Moreover, it is regarded as a marvelous material as it is mixed-valent with Mn vacancies within the lattice [27]. Incorporation of any transition metal ion into the Mn_3O_4 matrix can bring about significant improvement in its desired properties. Meanwhile, this work has been done to look into its capability to oxidize organic constituents in industrial waste water, which is an indispensable quality needed for a material to function as a photocatalyst.

Methylene blue is a heterocyclic organic dye with the molecular formula $C_{16}H_{18}N_3SCl$. It appears as an odourless dark green crystalline powder, stable in air. When dissolved in water gives a navy blue solution and spectrophotometric studies reveal that it has a characteristic absorbance peak at 653 nm. It is most commonly used dye in textile industries for coloring cotton, wood, paper stocks, and silk. It is also utilized in the field of medicine as a staining agent during surgery

* Corresponding author: priyam@saveetha.ac.in

or in other diagnostic exam. Constant exposure to methylene blue releases aromatic amines (e.g., Benzedrine, Methylene) which are potential carcinogens causing increased heart rate, shock, tissue necrosis, cyanosis and vomiting in humans. Due to its harmful effects, methylene blue should be eradicated from the human environment. Its presence, even in small amount is hazardous to aquatic life as it increases the Biochemical Oxygen Demand (BOD) level as well as affects the food web. Chemical structure of used methylene blue is shown in Fig.1 [28, 29].

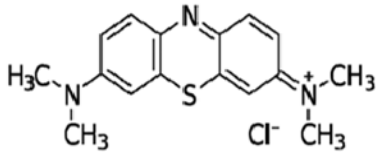

Fig. 1. Structure of Methylene Blue.

Comparative study of Pure and zinc doped Mn_3O_4 nanoparticles application in oxidation of methylene blue dye by photocatalytic decoloration has not been reported yet. Herein, we report a solid state synthesis of Pure Mn_3O_4nanoparticles and an approach to incorporate 3d transition metal (zinc) into Mn_3O_4 nanoparticles. The results obtained from various characterization techniques are explained in forthcoming paragraphs. The degradation efficiencies of the nanoparticles were studied with model organic dye methylene blue. A comparison of the photocatalytic property of all the samples is also presented.

2. Experimental procedure

2.1. Sample Preparation

Synthesis of Pure Mn_3O_4 nanoparticles was carried out at room temperature by simple chemical precipitation. Solution of 0.88 g of NaOH in 100 ml of distilled water was prepared in which 2.177 g of $MnCl_2.4H_2O$ was dissolved. To restrain the reunion of nanoparticles, 25 mg of Cetyl Tetra Methyl Ammonium Bromide (CTAB) as a surfactant was added with constant stirring. After 24 h stirring a brown color precipitate was obtained. The obtained precipitate was filtered, washed several times with double distilled waterand dried in a hot air oven at around 80 °C overnight. Calcination at 500 °C for 2h under air at a ramping rate of 5°C $min^{-1}$was done to remove the surfactant. Zinc doped Mn_3O_4nanocrystals were prepared using 0.38g of $KMnO_4$ and three different solutions containing 6, 12, 18 atomic percentages of zinc sulfate with respect to manganese were dissolved in 20 ml of deionized water at room temperature. Using an electronic balance relevant quantity of precursors were weighed according to the molar ratio. Gradual addition of 1.5 ml of absolute ethanol was carried out while the solution was vigorously stirred. The products were filtered, washed with double distilled water and absolute ethanol, dried at 70°C for 6 h followed by calcination at 120°C for 12hrs.

2.2. Characterization

The crystalline formation of Pure and zinc doped Mn_3O_4 nanoparticles were confirmed by powder X-ray diffraction studies. The X-ray powder patterns of these samples were recorded using Rigaku D/max-A X-ray diffractometer (CuKα, λ=1.5418 Å) at the scanning rate of 2 deg/min and 2θ is variedfrom10–70˚. Structure and morphology was examined by SEM, EDX and TEM. Specific surface area of all the samples were determined by BET (Brunauer–Emmett–Teller) analysis. The optical absorption measurements were made using a Lambda 35 UV Winlab Spectrometer, in the range of 190 - 1100nm. Photocatalytic studies were done to degrade methylene blue dye using 50mg of sample irradiated by Xe lamp (500 W).

3. Result and discussion

3.1. XRD analysis

The XRD pattern of Pure and Zn doped Mn_3O_4 nanoparticles are shown in Fig.2. It was used to identify the phase and purity of the prepared samples. The diffraction peak matches well with the reported tetragonal structure of Mn_3O_4 nanoparticles (JCPDS card no. 24-0734) [30]. In addition, there is no evidence for the presence of any other oxidation state of manganese, which indicates the high phase purity of the prepared Mn_3O_4 sample [31].The average crystallite size of all the prepared samples were calculated using Scherrer formula is shown in Table 1.

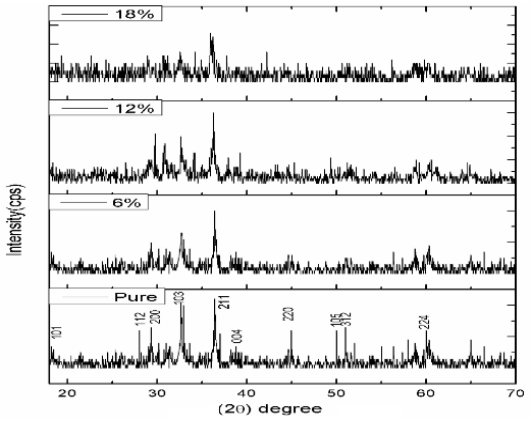

Fig. 2. XRD pattern of Pure, 6 at%, 12 at% and 18 at% of zinc doped Mn_3O_4 nanoparticles.

Table 1. Average crystallite size of all the prepared samples.

Zn concentrations (at%)	FWHM(β) (radians)	Average Crystallite size (nm)
Pure Mn_3O_4	0.1210	72.33
Mn_3O_{4+}6%	0.1302	67.22
Mn_3O_4 + 12%	0.1585	55.21
Mn_3O_4 +18%	0.2523	34.69

It is seen that the particle size is relatively small for all the doped samples when compared with the Pure and it is also decreasing with increase in concentration of Zn. XRD patterns of the products at different doping levels in Fig.1, evidently shows that the samples maintained good crystallinity up to 18 at% of doping and no extra peak was found due to Zn incorporation, which confirmed the proper phase formation of the materials. This also reveals that Zn is successfully doped in Mn_3O_4. As dopant concentration increases, broadening and intensity decrease of all diffraction peaks can be observed which indicates the formation of Mn_3O_4/Zn nanoparticles [32].

3.2. SEM and TEM analysis

To further confirm the influence of Zn in the nucleation and growth of Mn_3O_4, the formation and nature of the particles was recorded by scanning electron microscope (SEM) and transmission electron microscope (TEM). The structural morphology of 12at% Zn in Mn_3O_4 was recorded. Fig.3 (a, b) depicts the SEM images of 12at% Zn in Mn_3O_4 nanoparticles, taken at two different scanning ranges, which represents the sample contains spherical like structures.

The energy dispersive X-ray Analysis (EDX) spectrum (Fig. 3(c)) confirms the energy peaks are in congruence with the elements manganese, zinc and oxygen. It is clearly displayed that no other peak related to any impurity has been detected.

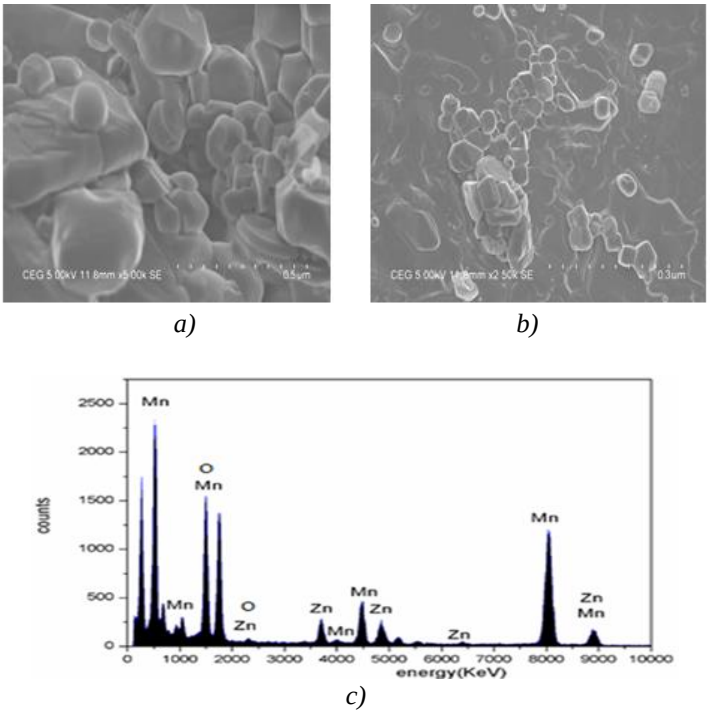

Fig. 3. (a) Magnification at 500 nm (b) Magnification at 300 nm (c) EDX spectrum of 12at % zinc doped Mn_3O_4 nanoparticles.

Moving in the clockwise direction of Fig.4, first two images are taken at two different magnifications of 100nm and 50nm which portrays that the particles are not only monodispersed but also uniform. Third image is the selective area electron diffraction (SAED) pattern of 12at% Zn in Mn_3O_4 nanoparticles and the fourth image is the lattice fringes of the Mn_3O_4, observed using the HRTEM image. By careful measurements, the lattice spacing is measured to 0.27nm, which corresponds to the <103> plane of Mn_3O_4 (JCPDS card No. 24-0734). Furthermore this observation was supported by the results from XRD data as explained.

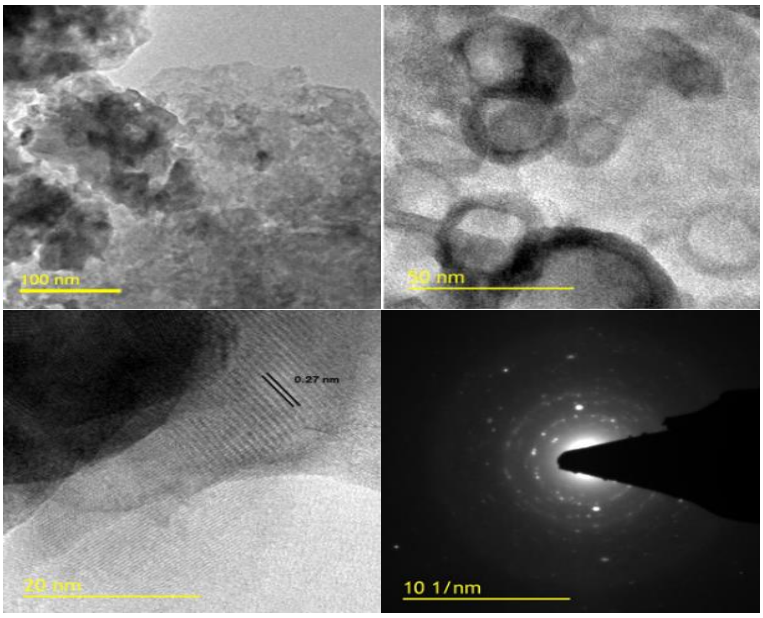

Fig. 4. TEM images of 12at% Zn in Mn_3O_4.

3.3. BET analysis

Adsorption-desorption isotherms for bare and doped Mn_3O_4 were studied by nitrogen adsorption-desorption Brunauer–Emmett–Teller (BET) analysis shown in Fig.5, to evaluate the surface area of the nanoparticles. It has been noticed that the hysteresis loop is identical to type IV adsorption-desorption curve. Evidently, the particles were found to be mesoporous in nature. The surface area of pure Mn_3O_4 and Mn_3O_4 contents with 6at%, 12at%, 18at% of Zn were calculated to be 15.03m^2g^{-1}, 33.16m^2g^{-1}, 46.32m^2g^{-1}, 40.16m^2g^{-1} respectively. Therefore, the specific surface area increases for the samples synthesized upto 12at% Zn and a subsequent decrease was observed for 18at% Zn. This might be due to small crystallite size of 18at% Zn in Mn_3O_4, which is apparent to XRD results listed in Table 1.

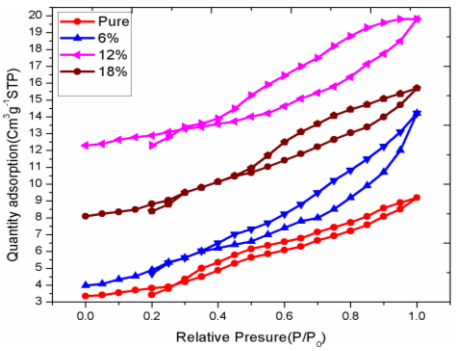

Fig. 5. Nitrogen adsorption-desorption isotherms of pure Mn_3O_4 and doped Mn_3O_4.

3.4. DRS Spectra

The energy band gap (E_g) is an important feature of oxides, which determines their applications in photocatalytic activity. However, for powder products, the scattering effect is enhanced, and Diffuse Reflectance Spectroscopy (DRS) is used desirably. The theory related to DRS spectra was proposed by Kubelka and Munk [33], which enables to obtain Eg of powder samples.UV-visible reflectance spectra of Pure and doped Mn_3O_4 is illustrated in Fig.6. The optical bandgap of Pure and doped Mn_3O_4 nanoparticles, were calculated using theKubelka–Munk function as follows [34-35].where $F(R_\infty)$ is the K–M function, $R_\infty$is the diffuse reflectance of an infinitely thick sample, $K(\lambda)$ is the absorption coefficient, s(λ) is the scattering coefficient, α is the linear absorption coefficient of the material, hν is the photon energy and E_g is the band gap energy. From the below equation the band gap energy was calculated by extrapolating the linear portion of the plots of $(F(R_\infty)h\nu)^{1/2}$ versus $(h\nu)$.

$$F(R_\infty)= \frac{(1-R_\infty)^2}{2R_\infty} = \frac{k(\lambda)}{s(\lambda)} \propto \alpha = \frac{(h\nu - Eg)^2}{h\nu} \quad (1)$$

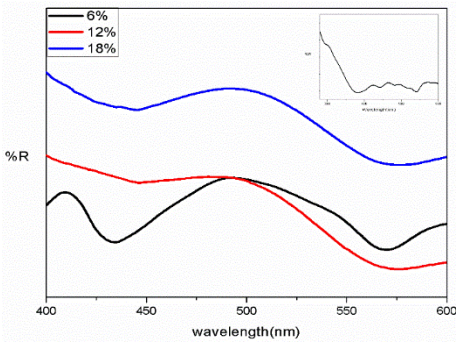

Fig. 6. UV Visible spectrum of 6 at%,12 at% and18 at% of zinc doped Mn_3O_4 nanoparticles (inset shows Pure Mn_3O_4 nanoparticles).

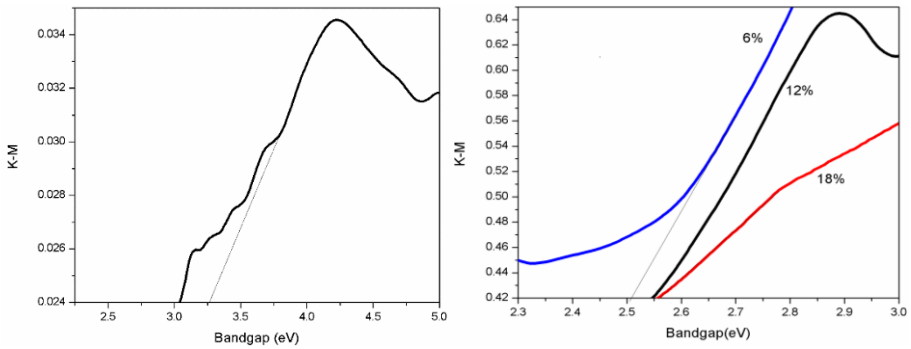

a) *b)*

Fig. 7. Band gap energies of a) PureMn_3O_4, and (b) zinc doped Mn_3O_4 nanoparticles with 6 at% 12 at% and 18 at%

.

The energy bandgaps for pure and doped samples have been illustrated in Fig. 7(a) and Fig. 7(b). From Fig.7 (a) we see that the value of the direct bandgap for Pure Mn_3O_4 is 3.26eVand the band gaps of 6, 12 and 18 at% were found to be 2.51eV, 2.54eV, 2.56eV. Perhaps, the bandgaps were found to be increasing with increase in concentration of Zn, which is shown in Fig. 7(b). Bandgap of all the doped samples is less than the Pure Mn_3O_4 additionally, they were found to be in the in the visible region. This might be due to the fact that during the reaction $KMnO_4$is reduced by ethanol to manganese whose oxidation state decreases from Mn^{7+}toMn^{3+}, as +3 state is a much stable state of manganese, very small amount of Mn gets further reduced to Mn^{2+} states. When Zn precursor was incorporated in the synthesis process, it influences the reduction process highly and on further increasing the doping percentage, it elevates the process of reduction of Mn to Mn^{2+} states thereby proliferating the formation of Mn_3O_4 nanoparticles. Due to the $3d^{10}$ electronic configuration Zn^{2+}cations are highly stabilized on the tetrahedral sites thereby substituting for Mn^{2+}tetrahedral cations. Red shift in the wavelength is observed due to structural change caused by doping [36].

3.5 Photocatalytic activity studies for MB dye degradation

3.5.1 Effect of time

For this study 1 x 10^{-4} M aqueous solution of methylene blue was used. 50 mg $L^{-1}$of each sample optimized as mentioned in the synthesis part was added. Before irradiation the system was magnetically stirred for 30minutes under dark to establish the adsorption-desorption equilibrium between the catalytic surface and the dye.

The irradiation time was done for 75 min. After the lamp was switched on, around 10ml of the suspension was pipetted out from the solution at an interval of 10 minutes. The pipetted sample was filtered and its absorbance was measured. Fig.8 shows the absorption spectrum of MB for (a) pure (b) 6 at% (c)12 at% (d) 18 at% of zinc doped Mn_3O_4 nanoparticles and it is observed that the absorption intensity of the peak at 653 nm for the MB dye decreased with increase in irradiation time which confirms progress of the degradation of the MB dye and all the samples were stable during the process. Fig.9 shows % degradation of methylene blue, by Pure, 6 at%, 12 at% and 18 at% of zinc doped Mn_3O_4nanoparticles.

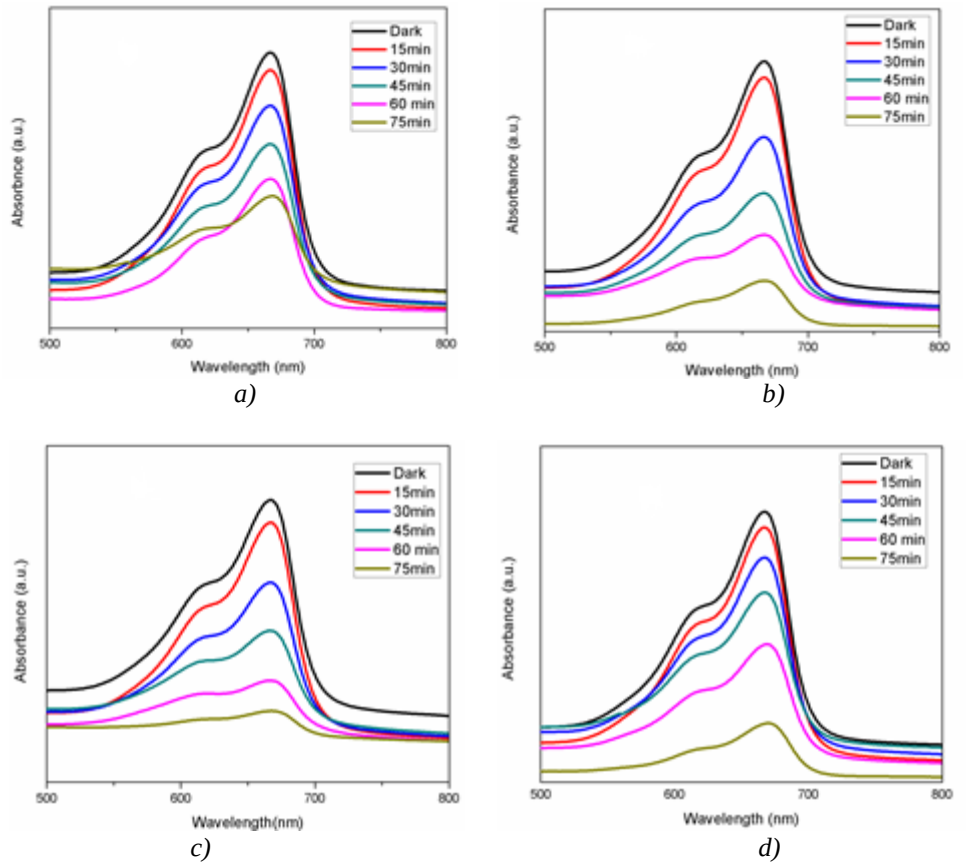

Fig. 8. Absorption spectrum of MB for (a) Pure (b) 6 at% (c) 12 at% (d)18 at% of zinc doped Mn_3O_4 nanoparticles.

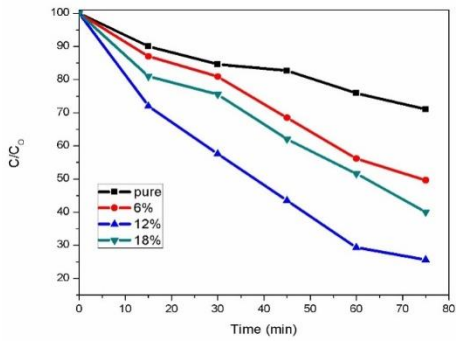

Fig. 9. %Degradation of MB against time, Pure, 6 at%, 12 at% and18 at% of zinc doped Mn_3O_4 nanoparticles.

3.5.2. Effect of dopant concentration

Studies involve 1 x 10^{-4} M aqueous solution of methylene blue, 50 mg L^{-1} of each sample and light illumination for seventy five minutes. The Pure and doped samples were used to evaluate their photocatalytic activity. The decoloration of MB was monitored by the UV–vis spectrometer and their degradation efficiencies were compared.

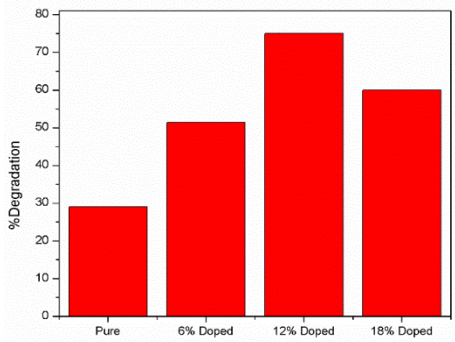

Fig. 10. % Degradation of MB against dopant concentration.

The degradation percentages were calculated by using the expression

$$\eta=(1-C/C_0)\times100 \quad (2)$$

where C_0 is the concentration of MB before illumination and C is the concentration after a certain irradiation time. The photo degradation activities of Mn_3O_4 with different concentrations of Zn were analyzed. The degradation efficiencies of Pure, 6, 12 at % were found to be 29%, 51%, 75%, and upon increasing the Zn concentration to 18at% the efficiency decreases to 60% respectively, as shown in Fig.10.This might be due to the fact that small particle size results in agglomeration at the surface, reducing the surface area which is in strong agreement with the results obtained from X-ray diffraction studies and BET analysis. Due to this reason, though the particle size is less for 18at% than 12 at%, the degradation efficiency of 12at% is more than 18at% [37-38]. Hence 12at% of Zn is an appropriate amount for the excellent photo degradation of MB and it was also observed that the photocatalytic degradation efficiency does not increase monotonously with the increase of Zn content. Therefore 12 at% Zn can be considered as the optimum weight percentage. The presence of Zn up to the optimum amount acts as electron–hole separation centre and hence upgrades the photocatalytic activity and when it is above 12 at%, Zn begins to act as a charge carrier recombination centre hence reduces the efficient charge separations. This presumably might also be another reason for less activity in 18at% Zn catalyst [39].

Owing to the fact that when the dopant concentration is 18 at%, the efficiency of charge separation decreases as the space charge region narrows which lowers the catalytic activity. 12 at% of Zn is found to be an ideal concentration of dopant ions which makes the thickness of space charge layer significantly equal to the light penetration depth. From the above observations we can come to a conclusion that when the quantity of doping ions is too high, the depletion region becomes very narrow and the penetration depth of light into Mn_3O_4 greatly exceeds the depletion region which makes the recombination of photo generated carriers easier [40]. To sum up, from the Fig.10, there is an optimum concentration which is 12at% of Zn in Mn_3O_4which has the most efficient separation of photo generated carriers and thereby photocatalytic activity.

3.5.3. Photocatalytic mechanism

When Zn doped Mn_3O_4 is exposed to visible light, photo generated electrons are excited from valence band to conduction band Eq3. From the conduction band, photoexcited electrons relocate to the surface of photocatalyst and their role is to capture adsorbed O_2 which upgrades the separation efficiency of charge carriers. Then $Zn^{2+}$is reduced to $Zn^{1+}$by electrons Eq4. Superoxide radical anions ($O_2^{\bullet-}$) are formed by the reaction between these electrons and dissolved oxygen in the system Eq5, which in turn result in the formation of hydroxyl radicals (•OH) Eq6. These •OH radicals are primarily responsible for the oxidation of the organic compounds Eq7. These two processes, increases the photocatalytic efficiency Eq8. Simultaneously more methylene blue molecules are adsorbed on the surface of the catalyst, enhancing the concentration of photo excited electrons to the conduction band and at the same time more number of electrons are transferred to the adsorbed O_2 [41]. Schematic representation of photo degradation of dye is shown in Fig.11.

$$Mn_3O_4 + h\nu \rightarrow Mn_3O_4 (e^-_{CB} + h^+_{VB}) \quad (3)$$

$$Zn^{2+} + e^- \leftrightarrow Zn^{1+} \quad (4)$$

$$e^-_{CB} + O_2 \rightarrow O_2^{-\bullet} \quad (5)$$

$$Mn^{3+} + OH^- \rightarrow Mn^{2+} + HO^\bullet \quad (6)$$

$$OH^- + h^+_{VB} \rightarrow HO^\bullet$$

$$H_2O + h^+_{VB} \rightarrow H^+ + OH^\bullet \quad (7)$$

$$H^+ + O_2^{-\bullet} \rightarrow HOO^\bullet$$

$$HOO^\bullet + HOO^\bullet \rightarrow H_2O_2 + O_2$$

$$H_2O_2 + O_2 \rightarrow O_2 + HO^\bullet + OH^- + O_2$$

$$H_2O_2 + HO^\bullet \rightarrow H_2O_2 + HOO^\bullet$$

$$O_2^{-\bullet} + HO^\bullet + MB \rightarrow \text{degradation products} \quad (8)$$

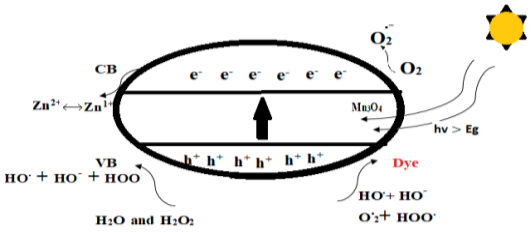

Fig. 11. Schematic representation of photo degradation of dye.

4. Conclusions

In the present study Pure Mn_3O_4 and different weight compositions of Mn_3O_4/Zn were successfully synthesized by simple chemical precipitation method and its structure, morphology, optical and photocatalytic properties were studied. The crystalline formation of all the synthesized samples were confirmed by powder X-ray diffraction studies and crystallite size of the samples were estimated around 30-70 nm using Scherrer equation. SEM, EDX and TEM images predicts plausible growth mechanism. Surface area values obtained from BET analysis play a major role as oxidative degradation took place via surface mechanism.

Optical absorption measurement results show that by doping impurity atoms, a red shift in the wavelength was observed which effectively shifted the photocatalytic activity from UV to visible light. From photocatalytic studies it is evident that the degradation efficiency of methylene blue treated with 12at% Zn in Mn_3O_4 is maximum when compared to other samples and it is also the optimum level beyond which there is no significant increase in decoloration of MB. Particle size, surface area and visible light sensitivity complements the superior oxidative capacity of 12at% Zn in Mn_3O_4. Overall, it can be concluded that Zn doped Mn_3O_4 nanoparticles can be suitable cost effective photocatalyst compatible with nature and environment, tailored to revive industrial waste water from effluents.

References

[1] M. He, L. Kang, C. Liu, Z. Lei, Z-H. Liu, Materials Research Bulletin **68**, 194 (2015).
[2] V. Štengl, J. Bludská, F. Opluštil, T. Němec, Materials Research Bulletin **46**(11),2050 (2011).
[3] M. Ni, M. K. H. Leung, D. Y. C. Leung, K. Sumathy, Sustain. Energy Rev **11**(3), 401 (2007).
[4] A. O. Ibhadon, P. Fitzpatrick, Recent Advances and Applications Catalysts **3**(1), 189 (2013).
[5] X. Gong, Y. Yang, S. Huang, Chem. Commun **47**(3), 1009 (2011).
[6] X. Li, L. Zhou, J. Gao, H. Miao, H. Zhang, J. Xu, Powder Technol **190**(3), 324 (2009).
[7] F. Qu, P. Vasilopoulos, Phys. Rev. B **74**(24), 245308 (2006).
[8] M. L. Singla, S. Awasthi, A. Srivastava, Sens. Actuators B **127**(2), 580 (2007).
[9] K. Majid, S. Awasthi, M. L. Singla, Sens. Actuators A **135**(1), 113 (2007).
[10] G. An, P. Yu, M. Xiao, Z. Liu, Z. Miao, K. Ding, L. Mao, Nanotechnology **19**(27), 275709 (2008).
[11] W. Wei, X. Cui, W. Chen, D. G. Ivey, Chem. Soc. Rev **40**(3), 1697 (2011).
[12] H. Jiang, T. Zhao, C. Yan, J. Ma, C. Li, Nanoscale **2**, 2195 (2010).
[13] C. Galindo, P. Jacques, A. Kalt, J. Photochem. Photobiol. A: Chem **130**(1), 35 (2000).
[14] Sridharan Balu, KasimayanUma, Guan-Ting Pan, Thomas C.-K. Yang, Sayee Kannan Ramaraj, Materials **11**, 1030 (2018).
[15] I. Arslan, I. A. Balcioglu, T. Tubkanen, Environ. Tech **20**(9), 921(1999).
[16] R. Asahi, T. Morikawa, T. Ohwaki, K. Aoki, Y. Taga, Science **293**(5528), 269 (2001).
[17] Vassilios Binas, DanaeVenieri, Dimitrios Kotzias, George Kiriakidis, Journal of Materiomics **3**(1), 3 (2017).
[18] K. Rajalakshmi, V. Jeyalakshmi, K. R. Krishnamurthy, B. Viswanathan, Indian Journal of Chemistry **51**(03), 411 (2012).
[19] G. Colon, M. C. Hidalgo, J. A. Navio, J. Photochem. Photobiol. A: Chem **138**(1), 79 (2001).
[20] Hongxiang Fu, Gongxuan Lu, ShubenLi, J. Photochem. Photobiol. A: Chem **114**(1),81(1998).
[21] A. Fujishima, T. N. Rao, D. ATyrk, Photochemistry Reviews **1**(1), 1 (2000).
[22] Y. Zhu, L. Zhang, W. Yao, L. Cao, Appl. Surf. Sci **158**(1-2), 32 (2000).
[23] Y. Zhu, L. Zhang, L. Wang, Y. Fu, L. Cao, J. Mater. Chem **11**(7), 1864 (2001).
[24] S. K. Zheng, T. M. Wang, W. C. Hao, R. Shen, Vaccum **65**(2), 155 (2002).
[25] S. P. Adhikariand, A. Lachgar, J. Phys.: Conf. Ser. **758**, 012017 (2016).
[26] Zhang Li, Y. Zhu, Y. He, W. Li, H .Sun, Appl. Catal. B: Environ **40**(4), 287 (2003).
[27] K. A. M. Ahmed, K. Huang, Arabian Journal of Chemistry **13**(1), 2785 (2020).
[28] Beyza Cabir, Mehmet Yurderi, Nurdan Caner, Mehmet Salih Agirtas, Mehmet Zahmakiran, Murat Kaya, Materials Science and Engineering: B **224**, 9 (2017).
[29] M. R. Bayati, F. Golestani-Fard, A. Z. Moshfegh, Catal. Lett **134**, 162 (2010).
[30] G. An, P. Yu, M. Xiao, Z. Liu, Z. Miao, K. Ding, L. Mao, Nanotechnology **19**(27), 275709 (2008).
[31] Y. Li, H. Tan, X. Y. Yan, B. Goris, J. Verbeeck, S. Bals, P. Colson, R. Cloots, G. V. Tendeloo, B. L. Su, Small **7**(4), 475 (2011).
[32] K. J. Kim, Y. R. Park, J. Cryst. Growth **270**(1-2), 162 (2004).
[33] P. Kubelka, F. Munk, Z. Tech. Phys **12**, 593 (1931).
[34] P. Muralimanohar, R. Parasuraman, J. Rajeev Gandhi, M. Rathnakumari, P. Sureshkumar, Optik **127**(20), 8956 (2016).
[35] Angamuthuraj Chithambararaj, Arumugam Chandra Bose, Beilstein J. Nanotechnology **2**, 585 (2011).
[36] J. B. Goodenough, A. L. Loeb, Phys. Rev **98**(2), 391 (1955).
[37] A. C. Dodd, A. J. McKinley, M. Saunders, T. Tsuzuki, J. Nanoparticle Res. **8**, 43 (2006).
[38] X. Li, Q. Li, L. Wang, Phys. Chem. Chem. Phys **15**(34), 14282 (2013).
[39] W. Wu, R. Lin, L. Shen, R. Liang, R. Yuan, L. Wu, Catal. Commun **40**, 1 (2013).
[40] K. Imamura, S. Iwasaki, T. Maeda, K. Hashimoto, B. Ohtani, H. Kominami Phys. Chem. Chem.Phys **13**(11), 5114 (2011).
[41] W. Wu, G. Liu, S. Liang, Y. Chen, L. Shen, H. Zheng, R. Yuan, Y. Hou, L. Wu, J. Catal **290**, 13 (2012).